Josephson effect between a two-band superconductor with $s++$ or $s\pm$ pairing symmetry and a conventional s-wave superconductor

Shi-Zeng Lin[*]

Theoretical Division, Los Alamos National Laboratory, Los Alamos, New Mexico 87545, USA
(Received 9 April 2012; published 11 July 2012)

In this work, we investigate the Josephson effect between a two-band superconductor either with the $s++$ (two energy gaps have the same sign and are fully gapped) pairing symmetry or $s\pm$ (two energy gaps have π phase difference and are fully gapped) pairing symmetry and a conventional s-wave superconductor. The ground state, critical current, plasma modes, flux-flow dynamics, response to external ac electric field, and possible soliton solutions are investigated. For junctions with the charge neutrality breaking, we find a new plasma mode for junctions, which gives rise to new resonance peaks in the Josephson flux-flow region. Because of the frustrated interaction in junctions with $s\pm$ pairing symmetry, time-reversal symmetry (TRS) can be broken if the frustration is optimized. In the TRS broken (TRSB) state, there is a nontrivial phase difference between the two Josephson tunneling channels, which results in a nontrivial interference. Furthermore, we find a massless plasma mode at the TRSB transition for junctions with the charge neutrality breaking. In the TRSB state, a spontaneous magnetic flux appears where there is a spatial inhomogeneity in the Josephson coupling, thus providing a possible smoking-gun evidence for the underlying pairing symmetry.

I. INTRODUCTION

The Josephson effect between two superconductors is a hallmark of the macroscopic quantum effect associated with superconductivity.[1] When a phase difference exists between two conventional superconductors, spontaneous supercurrent flows from one superconductor to the other when they are brought together to form a Josephson junction. This is the celebrated dc Josephson effect which describes the relation between the current and phase difference $I_s = I_c \sin(\theta_1 - \theta_2)$, where I_c is the critical current and θ_i is the superconducting phase. When a voltage V is applied to the junction, the superconducting phase rotates according to the ac Josephson effect $\hbar\partial_t(\theta_1 - \theta_2) = 2 \, eV$. Because of the novel quantum nature of the Josephson effect, Josephson junctions have wide applications, such as SQUID, electromagnetic devices, and quantum qubit.[2]

The Josephson effect involving the phase of the superconductivity therefore depends sensitively on the underlying pairing symmetry of the superconductors. Thus, the Josephson effect provides an invaluable tool to pin down the pairing symmetry of some exotic superconductors, such as Geshkenbein, Larkin, and Barone phase sensitive measurement for p-wave pairing symmetry in heavy-fermion superconductors,[3] and trijunction in cuprate superconductors.[4] On the other hand, the current-phase relation is modified in these exotic junctions,[5] which broadens our general understanding on the Josephson effect and also points to a new possible direction for applications.

The multiband superconductivity attracts considerable interests since the discoveries of the MgB_2 superconductor[6] and iron pnictide superconductors.[7] The pairing symmetry in MgB_2 now is well understood. It has two s-wave energy gaps with the same phase in the σ and π bands, known as $s++$ pairing symmetry.[8] While for pnictide superconductors, due to the vastness of the iron pnictide family, discrepancies from different measurements and controversies remain (see

Refs. 9–15 for a review). The so-called extended s-wave or $s\pm$ pairing symmetry with a π phase shift between the hole and electron Fermi surface[16,17] has attracted considerable attention and is favored by many experiments[18–21] and is considered as a most probable candidate for iron pnictide superconductors.

Soon after the discoveries of iron pnictide superconductors, Josephson junctions have been fabricated between a conventional superconductor and these multiband superconductors, with an aim to determine the pairing symmetry of pnictide. Zhang *et al*.[22] fabricated a junction between BaKFeAs and a conventional superconductor Pb, and they clearly observed the Fraunhofer pattern in the dependence of the critical current on magnetic fields and Shapiro steps when the junction is irradiated by microwaves. These observations indicate that a pure p-wave or d-wave pairing symmetry is unlikely realized in pnictide. Similar Fraunhofer pattern is observed by Zhou *et al*. in a corner junction between BaFeCoAs and Pb.[23] Recently, unambiguous half-integer flux quantum jumps have been observed in polycrystal NdFesO-niobium superconducting loop,[24] which is a strong evidence for the $s\pm$ pairing symmetry. For a review on MgB_2 junctions and all pnictide junctions, please see Refs. 25–27.

From a theoretical point view, for Josephson junctions between two-band superconductors and conventional s-wave superconductors, there are two superconducting tunneling channels $J_{s1} \sin(\theta_1 - \theta_s)$ and $J_{s2} \sin(\theta_2 - \theta_s)$, where θ_s is the phase of the s-wave superconductor and θ_i with $i = 1,2$ is the phase of the two-band superconductor. The relative phase between θ_1 and θ_2 is fixed by the underlying pairing symmetry. For the $s++$ pairing symmetry, such as MgB_2, these two channels have the same phase and add constructively, thus the phase-current relation is equivalent to a conventional junction made of single-band superconductors with an effective Josephson coupling $J_{\text{eff}} = J_{s1} + J_{s2}$. While, for the $s\pm$ pairing symmetry, nontrivial phenomena unique to the sign-reversal pairing symmetry arise. It was discussed by Agterberg *et al*.[28] even before the discovery of pnictide superconductors that
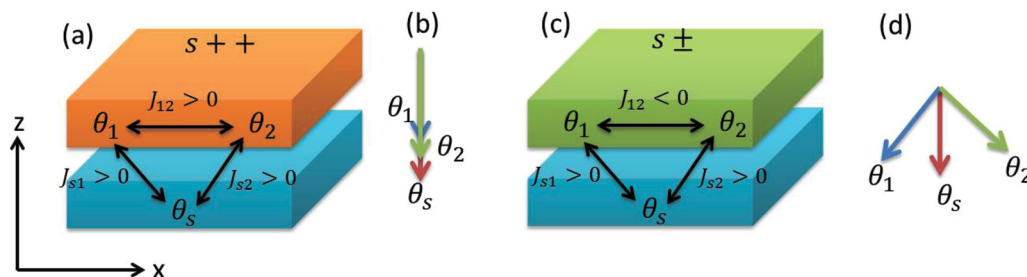
FIG. 1. (Color online) (a) Josephson junctions between two-band superconductors with the $s++$ pairing symmetry and s-wave single-band superconductors. The interaction between condensates is attractive and they have the same phase in the ground state as shown in (b). (c) Josephson junctions between two-band superconductors with the $s\pm$ pairing symmetry and s-wave single-band superconductors. The interaction between condensates θ_1 and θ_2 is repulsive. Under appropriate conditions, the system is strongly frustrated, resulting in TRSB, and the ground state is depicted in (d).

the critical current depends nonmonotonically on temperatures, and may even become negative in some temperature region. Assuming a π phase shift between the two tunneling channels, numerous phenomena have been demonstrated such as realization of the π junction,[29,30] vortex enlargement,[31] new Shapiro steps,[32] and upper bound of the critical current from the Ambegaokar-Baratoff relation.[33] We note that the most studies only show quantitatively the difference between junctions with $s++$ and $s\pm$ pairing symmetry.

Due to the $s\pm$ pairing symmetry, the system is somewhat frustrated as shown in Fig. 1(d). Nontrivial phase difference between two tunneling channels beside 0 with an effective Josephson coupling $J_{s1} + J_{s2}$ and π with an effective Josephson coupling $J_{s1} - J_{s2}$ is possible. If this happens, time-reversal symmetry (TRS) is broken and there are two degenerate ground states. The possible violation of TRS is first discussed in Ref. 34 and later in Ref. 35 in the context of three-band superconductors. As a consequence of time-reversal-symmetry breaking (TRSB), qualitatively different behavior between junctions made of $s\pm$ and $s++$ superconductors may exist, which is hopeful to resolve the dispute of the pairing symmetry in pnictide superconductors by observing the differences in experiments.

In this work, we investigate the Josephson effect between a two-band superconductor with either $s++$ or $s\pm$ pairing symmetry and a conventional s-wave superconductor, with an emphasis on the possible TRSB. First, we derive equations of motion for the gauge-invariant phase differences based on the Lagrangian approach. Then, the ground state is obtained by minimizing the Josephson energy. We find that for junctions with $s\pm$ pairing symmetry under appropriate conditions, TRSB occurs. As a consequence of the TRSB, the critical current and height of the Shapiro step when junction is shined by an ac electric field develop a nontrivial phase dependence on the Josephson coupling. We proceed to investigate the Josephson plasma mode in junctions. For thin superconducting electrodes, charge neutrality breaking occurs, resulting in a modified ac Josephson relation. A new plasma dispersion associated with an out-of-phase oscillation of phase difference emerges. At the TRSB transition, this new plasma mode becomes massless. Because of the existence of the massless mode, the Josephson penetration depth diverges and the lower critical field H_{c1} of the junction vanishes. In the flux-flow region, we obtain additional Fiske resonances for a

given cavity index and an additional Eck resonance because of the charge neutrality breaking.

In the last part of the paper, we discuss possible topological excitations in the junction because of the existence of multiple degenerate energy minima. In the TRSB state, a new type of soliton can be stabilized between the TRSB pair states. Finally, we discuss the appearance of spontaneous magnetic flux when there is a spatial variation of the Josephson coupling, which occurs only in the junction with $s\pm$ pairing symmetry, thus providing a possible smoking-gun evidence for the pairing symmetry.

The remaining part of the paper is organized as follows: In Sec. II, we derive equations of motion for the gauge-invariant phase differences. In Sec. III, the boundary condition is derived. In Sec. IV, we calculate the phase differences at the ground state. In Sec. V, the dependence of the critical current on magnetic fields is obtained. In Sec. VI, the response of the junction to an incident electromagnetic wave is investigated. In Sec. VII, we calculate the Josephson plasma modes in the junction. In Sec. VIII, the Josephson penetration depth and the lower critical field are studied. In Sec. IX, the McCumber solution is obtained. In Sec. X, we investigate the Fiske and Eck resonances in the flux-flow region. In Sec. XI, we discuss the topological excitations (soliton) in the junction. In Sec. XII, possible spontaneous magnetic flux is investigated for junctions made of superconductors with $s\pm$ pairing symmetry. The paper is closed by conclusions in Sec. XIII.

II. MODEL

We consider a junction between a conventional s-wave superconductor and a multiband superconductor either with $s++$ or $s\pm$ pairing symmetry, as depicted in Fig. 1. The analysis can be extended straightforwardly to junctions between two two-band superconductors. However, the physics is expected to be qualitatively the same as the heterotic junctions studied here. In the junction between a $s++$ superconductor and a s-wave superconductor, the Josephson couplings among different condensates are positive, thus in the ground state they have the same phase. While for the junction between a $s\pm$ superconductor and a s-wave superconductor, the interband Josephson coupling between condensates with phase θ_1 and θ_2 in the $s\pm$ superconductor is negative, and the interjunction Josephson coupling between the s-wave superconductor and

$s\pm$ superconductor is positive, which results in frustration in the system. When the frustration is optimized, different condensates have nonzero phase differences among them, which indicates the breaking of TRS. We will show below that the behavior is qualitatively different for junctions in Fig. 1(a) with TRS and Fig. 1(c) with TRSB, which implies a possible way to detect the pairing symmetry for multiband superconductors.

The Hamiltonian of the junction is

$$\mathcal{H} = \mathcal{H}_1 + \mathcal{H}_2 + \mathcal{H}_t, \tag{1}$$

with the Hamiltonian for the single-band superconductor

$$\mathcal{H}_1 = \int d^3r \sum_{\sigma} c_\sigma^\dagger(\mathbf{r})(\varepsilon_c - \mu_c)c_\sigma(\mathbf{r})$$
$$- g c_\sigma^\dagger(\mathbf{r})c_{\bar\sigma}^\dagger(\mathbf{r})c_{\bar\sigma}(\mathbf{r})c_\sigma(\mathbf{r}), \tag{2}$$

and the Hamiltonian for the two-band superconductor

$$\mathcal{H}_2 = \sum_{l,\sigma} \int d^3r\, d_{l\sigma}^\dagger(\mathbf{r})(\varepsilon_{d,l} - \mu_d)d_{l\sigma}(\mathbf{r})$$
$$- \sum_{j,l=1,2} \int d^3r\, d_{j\sigma}^\dagger(\mathbf{r})d_{j\bar\sigma}^\dagger(\mathbf{r})V_{jl}d_{l\bar\sigma}(\mathbf{r})d_{l\sigma}(\mathbf{r}), \tag{3}$$

and the tunneling between the two superconductors

$$\mathcal{H}_t = \sum_{l,\sigma} t_{l,s} c_\sigma^\dagger d_{l\sigma} + \text{H.c.}, \tag{4}$$

where $d_{l\sigma}^\dagger$ ($d_{l\sigma}$) is the electron creation (annihilation) operator in the lth band of the two-band superconductor with the dispersion $\varepsilon_{d,l}(\mathbf{k})$ and the chemical potential μ_d and spin index σ. V_{jl} is the intraband for $l = j$ and interband for $l \neq j$ scattering, respectively, which can be either repulsive or attractive depending, for instance, on the strength of the Coulomb and electron-phonon interaction. $c_\sigma^\dagger$ is the electron creation operator in the single-band superconductor and g is the electron-phonon coupling strength. $t_{l,s}$ is the tunneling matrix for electrons between the two superconductors.

A schematic view of the junction geometry is depicted in Fig. 1. External magnetic fields are applied along the y direction, which induces inhomogeneous phase differences along the x direction. We assume that the system is uniform along the y direction and the problem becomes two dimensional. We proceed to derive equations of motion for the gauge-invariant phase differences for the junction using the Lagrangian approach.[36,37] The total Lagrangian of the system has three contributions

$$\mathcal{L} = \mathcal{L}_1 + \mathcal{L}_2 + \mathcal{L}_B \tag{5}$$

with the Lagrangian for the single-band superconductor, which can be derived from the Hamiltonian equation (2) using a standard method[38]

$$\mathcal{L}_1 = \frac{d}{8\pi\mu_s^2}\left[A_0^B(r) + \frac{\Phi_0}{2\pi c}\partial_t\theta_s(r,t)\right]^2$$
$$- \frac{d}{8\pi\lambda_s^2}\left[A_x^B(r) - \frac{\Phi_0}{2\pi}\nabla\theta_s(r,t)\right]^2 \tag{6}$$

and the Lagrangian the two-band superconductor

$$\mathcal{L}_2 = \sum_{i=1,2} \frac{d}{8\pi\mu_i^2}\left[A_0^T(r) + \frac{\Phi_0}{2\pi c}\partial_t\theta_i(r,t)\right]^2$$
$$- \sum_{i=1,2} \frac{d}{8\pi\lambda_i^2}\left[A_x^T(r) - \frac{\Phi_0}{2\pi}\partial_x\theta_i(r,t)\right]^2$$
$$+ \frac{J_{12}\Phi_0}{2\pi c}\cos(\theta_1 - \theta_2), \tag{7}$$

where μ_s and μ_i are the Thomas-Fermi lengths associated with charge screening, and λ_s and λ_i are the penetration depths for each band, and θ_s and θ_i are the superconducting phases for different condensates, respectively. The effective penetration depth for the two-band superconductor is $\lambda_L^{-2} = \lambda_1^{-2} + \lambda_2^{-2}$. J_{12} is the interband Josephson coupling, and $J_{12} < 0$ for the $s\pm$ pairing symmetry while $J_{12} > 0$ for the $s{++}$ pairing symmetry. A_0^B and A_0^T are electric potentials, and A_x^B and A_x^T are vector potentials at the bottom and top electrodes. $\Phi_0 = hc/2e$ is the quantum flux. Here, we have introduced the charge energy [the first term at the right-hand side of Eqs. (6) and (7)] in the superconductors to account for the possible charge neutrality breaking[39–41] when the thickness of superconducting electrodes d is comparable to μ_s or μ_i, which might be realized in layered superconductors with strong anisotropy.[42]

The Lagrangian for the insulating barrier reads as

$$\mathcal{L}_B = \frac{b\epsilon_b}{8\pi}E_{b,z}^2 - \frac{b}{8\pi}B_{b,y}^2 - V_J, \tag{8}$$

with b being the thickness of the barrier and ϵ_d the dielectric constant. The electric field in the barrier is

$$E_{b,z} = -\frac{1}{c}\partial_t A_{b,z} - \partial_z A_0 = -\frac{1}{c}\partial_t A_{b,z} - \frac{A_0^T - A_0^B}{b}, \tag{9}$$

and the magnetic field is

$$B_{b,y} = \partial_z A_x - \partial_x A_{b,z} = \frac{A_x^T - A_x^B}{b} - \partial_x A_{b,z}. \tag{10}$$

The Josephson coupling V_J is

$$V_J = -\frac{J_{s1}\Phi_0}{2\pi c}\cos(\phi_{s1}) - \frac{J_{s2}\Phi_0}{2\pi c}\cos(\phi_{s2}), \tag{11}$$

with the gauge-invariant phase difference

$$\phi_{si} \equiv \theta_i - \theta_s - \frac{2\pi b}{\Phi_0}A_{b,z}, \tag{12}$$

with $i = 1, 2$ and $\theta_1 - \theta_2 = \phi_{s1} - \phi_{s2}$. Here, $J_{si} > 0$ are the Josephson couplings and can be derived from a microscopic theory[2]

$$J_{si} = \frac{2\hbar}{eR_{bi}}\frac{|\Delta_i\Delta_s|}{|\Delta_s| + |\Delta_i|}K\left(\frac{|\Delta_i| - |\Delta_s|}{|\Delta_i| + |\Delta_s|}\right) \tag{13}$$

for a temperature much smaller than the critical temperature, where $K(x)$ is the complete elliptic integral of the first kind, and Δ_s, Δ_i are the superconducting energy gaps for different condensates. The resistance for each channel at the barrier is

$$R_{bi} = \frac{\hbar^3}{4\pi}\frac{1}{e^2 N_i(0)N_s(0)t_{i,s}}, \tag{14}$$

where $N_i(0)$ is the density of state of quasiparticles in each band for the two-band superconductor and $N_s(0)$ is the density

of state for the single-band superconductor. The Josephson couplings depend on the resistance of the barrier for each channel R_{bi} and temperature, which implies a practical way of tuning in experiments.[28,43]

For convenience, we introduce a length $\lambda_{c1} = \sqrt{c\Phi_0/(8\pi^2 bJ_{s1})}$ and a frequency $\omega_{p1} = c/(\sqrt{\epsilon_d}\lambda_{c1})$. We then renormalize the length in units of λ_{c1} and time in units of $1/\omega_{p1}$. Current density is in units of J_{s1}, electric field is in units of $\Phi_0\omega_{p1}/(2\pi cb)$, and magnetic field is in units of $\Phi_0/(2\pi\lambda_{c1}b)$.

We then minimize the Lagrangian in Eq. (5) using the Euler-Lagrange equation. By applying the Euler-Lagrange equation with respect to A_0^T and A_0^B, we have

$$\sum_{i=1,2} \frac{1}{\alpha_i}\left[A_0^T + \partial_t\theta_i\right] - \epsilon_b\left[-b\partial_t A_b^z - \left(A_0^T - A_0^B\right)\right] = 0, \quad (15)$$

$$\frac{1}{\alpha_s}\left[A_0^B + \partial_t\theta_s\right] + \epsilon_b\left[-b\partial_t A_b^z - \left(A_0^T - A_0^B\right)\right] = 0, \quad (16)$$

where $\alpha_{s(i)} \equiv u_{s(i)}^2/(db)$ are parameters characterizing the importance of the charge neutrality breaking. Equations (15) and (16) can be combined into the following equation using Eqs. (9) and (12):

$$\sum_{i=1,2} \frac{\partial_t\phi_{\mathrm{si}}}{\alpha_i} = \left[\left(1 + \frac{\alpha_s}{\alpha_1} + \frac{\alpha_s}{\alpha_2}\right)\epsilon_b + \frac{1}{\alpha_1} + \frac{1}{\alpha_2}\right]E_{b,z}$$
$$\equiv C_e E_{b,z}. \quad (17)$$

Equation (17) is a modified ac Josephson relation as a result of charge neutrality breaking. In the limit $\alpha_i \to 0$, we recover the standard ac Josephson relation $\partial_t\phi_{si} = E_{b,z}$. We will show that a new plasma mode emerges for nonzero α_i and α_s.

Similarly, by minimizing the Lagrangian with respect to A_x^T and A_x^B, we have

$$-\sum_{i=1,2} \frac{1}{\zeta_i}\left[A_x^T - \partial_x\theta_i\right] - \left(A_x^T - A_x^B - b\partial_x A_z\right) = 0, \quad (18)$$

$$-\frac{1}{\zeta_s}\left[A_x^B - \partial_x\theta_s\right] + \left(A_x^T - A_x^B - b\partial_x A_z\right) = 0, \quad (19)$$

where $\zeta_{s(i)} \equiv \lambda_{s(i)}^2/(db)$. We then have the relation between the magnetic field and spatial derivative of the gauge-invariant phase difference after rewriting Eqs. (18) and (19) using

Eqs. (10) and (12):

$$\sum_{i=1,2} \frac{\partial_x\phi_{\mathrm{si}}}{\zeta_i} = \left[\left(1 + \frac{\zeta_s}{\zeta_1} + \frac{\zeta_s}{\zeta_2}\right) + \frac{1}{\zeta_1} + \frac{1}{\zeta_2}\right]B_{b,y} \equiv C_b B_{b,y}. \quad (20)$$

Equation (20) is a generalization of the phase magnetic field relation in junctions between two single-band superconductors. In Josephson junctions made of multiband superconductors, there exist fractional Josephson vortices according to Eq. (20), as will be discussed in Sec. XI.

By applying the Euler-Lagrangian equation with respect to $A_{b,z}$, we obtain the Ampere's law

$$\partial_x B_{b,y} = \sin\phi_{s1} + J_{s2}\sin\phi_{s2} + \partial_t E_{b,y}. \quad (21)$$

The interband Josephson current $J_{12}\sin(\phi_{s1} - \phi_{s2})$ does not enter because it does not couple with the gauge field. With the help of Eqs. (17) and (20), we then arrive at the first equation for the gauge-invariant phase difference ϕ_{si}:

$$\frac{1}{C_b}\left(\frac{\partial_x^2\phi_{s1}}{\zeta_1} + \frac{\partial_x^2\phi_{s2}}{\zeta_2}\right)$$
$$= \sin\phi_{s1} + J_{s2}\sin\phi_{s2} + \frac{1}{C_e}\left(\frac{\partial_t^2\phi_{s1}}{\alpha_1} + \frac{\partial_t^2\phi_{s2}}{\alpha_2}\right). \quad (22)$$

We still need one more equation for the gauge-invariant phase difference. This can be derived by variation of $\mathcal{L}$ with respect to θ_i and θ_s, which yields

$$-\frac{1}{\epsilon_b\alpha_s}\partial_t\left[A_0^L(r) + \partial_t\theta_s\right] - \frac{1}{\zeta_s}\partial_x\left[A_x^L - \partial_x\theta_s\right]$$
$$+ \sin\phi_{s1} + J_{s2}\sin\phi_{s2} = 0, \quad (23)$$

$$-\frac{1}{\epsilon_b\alpha_1}\partial_t\left[A_0^R(r) + \partial_t\theta_1\right] - \frac{1}{\zeta_1}\partial_x\left[A_x^R - \partial_x\theta_1\right]$$
$$- \sin\phi_{s1} - J_{12}\sin\phi_{12} = 0, \quad (24)$$

$$-\frac{1}{\epsilon_b\alpha_2}\partial_t\left[A_0^R(r) + \partial_t\theta_2\right] - \frac{1}{\zeta_2}\partial_x\left[A_x^R - \partial_x\theta_2\right]$$
$$- J_{s2}\sin\phi_{s2} + J_{12}\sin\phi_{12} = 0. \quad (25)$$

By subtracting $\zeta_1/\zeta_s\times$ Eq. (24) from Eq. (23), and using $A_0^B(r) + \partial_t\theta_s = -\alpha_s\epsilon_b E_b$, we obtain another equation for phases

$$-\left(\frac{\zeta_1}{\zeta_s}\frac{1}{\epsilon_b\alpha_1} + \frac{\zeta_1}{\zeta_s}\frac{\alpha_s}{\alpha_1} - 1\right)\frac{1}{C_e}\left(\frac{1}{\alpha_1}\partial_t^2\phi_{s1} + \frac{1}{\alpha_2}\partial_t^2\phi_{s2}\right) + \frac{\zeta_1}{\zeta_s}\frac{1}{\epsilon_b\alpha_1}\partial_t^2\phi_{s1} - \frac{1}{\zeta_s}\left[-\frac{1}{C_b}\left(\frac{1}{\zeta_1}\partial_x^2\phi_{s1} + \frac{1}{\zeta_2}\partial_x^2\phi_{s2}\right) + \partial_x^2\phi_{s1}\right]$$
$$+ \sin\phi_{s1} + J_{s2}\sin\phi_{s2} + \frac{\zeta_1}{\zeta_s}\left[\sin\phi_{s1} + J_{12}\sin(\phi_{s1} - \phi_{s2})\right] = 0. \quad (26)$$

Equations (21) and (26) together with boundary condition (derived below) completely describe the phase dynamics in the junction. In the limit of no charge neutrality breaking, $\alpha \to 0$, $\partial_t\phi_{si} = E_{b,z}$. When $|J_{12}| \gg J_{si}$, we have $\phi_{s1} = \phi_{s2}$ for $J_{12} > 0$ ($s++$ pairing symmetry) and $\phi_{s1} = \phi_{s2} + \pi$ for $J_{12} < 0$ ($s\pm$ pairing symmetry). In these limits, the dynamics of the junction reduces to a single junction version

$$\lambda_e^2\partial_x^2\phi_{s1} = J_e\sin\phi_{s1} + \partial_t^2\phi_{s1}, \quad (27)$$

with an effect Josephson coupling $J_e = 1 + \mathrm{sign}(J_{12})J_{s2}$ and an effective penetration depth $\lambda_e = \sqrt{(\zeta_1^{-1} + \zeta_2^{-1})/C_b}$, where $\mathrm{sign}[x] = -1$ for $x < 0$ and $\mathrm{sign}[x] = 1$ for $x > 0$. Here, J_e is negative for $J_{s2} < J_{s1}$ for $s\pm$ pairing symmetry, and Eq. (27) describes the phase dynamics in a π junction.[29,30,43,44] However, if we express the dynamical equation in terms of ϕ_{s2}, the sign of the Josephson current becomes positive and we have a conventional Josephson junction.

Dissipations can be introduced through a dissipation function

$$\mathcal{D} = \tfrac{1}{2}\beta_d E_b^2, \qquad (28)$$

where β_d is a damping coefficient. The equation of motion in the presence of dissipation can be derived similarly, using the Euler-Lagrange equation with dissipation

$$\frac{\delta\mathcal{L}}{\delta\theta_i} - \frac{\partial}{\partial x}\left[\frac{\delta\mathcal{L}}{\delta(\partial_x\theta_i)}\right] - \frac{\partial}{\partial t}\left[\frac{\delta\mathcal{L}}{\delta(\partial_t\theta_i)}\right] = \frac{\delta\mathcal{D}}{\delta(\partial_t\theta_i)}. \quad (29)$$

III. BOUNDARY CONDITION

Boundary conditions are crucial to determine the dynamics inside the junction. For a conventional single-band junction, the boundary condition is given by $\partial_x\phi = 2\pi B_a(2\lambda + b)/\Phi_0$ because the radiation effect is weak,[45] where B_a is the applied field and λ is the penetration depth. The boundary condition for the multiband junctions can not be generalized straightforwardly from single-band cases. Using the Usadel equation, the boundary condition for multiband superconductors is developed in Ref. 46. In this work, we assume that the supercurrent for each band vanishes at the left and right boundaries of the two-band superconductor, as shown in Fig. 1, and we have

$$\left(A_x^T - \frac{\Phi_0}{2\pi}\partial_x\theta_1\right) = \left(A_x^T - \frac{\Phi_0}{2\pi}\partial_x\theta_2\right) = 0, \quad (30)$$

which yields $\partial_x\phi_{s1} = \partial_x\phi_{s2}$ at the boundary using Eq. (12). Then, from Eq. (20), we derive the boundary condition

$$\partial_x\phi_{s1} = \partial_x\phi_{s2} = \frac{C_b}{\zeta_1^{-1} + \zeta_2^{-1}}\left(B_a \pm LJ_{\text{ext}}/2\right), \quad (31)$$

where J_{ext} is the bias current and L is the length of the junction. The second term in the parentheses at the right-hand side of Eq. (31) accounts for the magnetic field induced by the bias current. The magnetic field inside the junction $B_{b,y}$ is different from the applied magnetic field B_a due to the screening by Josephson current.

IV. GROUND STATE

In the absence of applied magnetic fields $B_a = 0$ and bias current $J_{\text{ext}} = 0$, the ground state is determined by minimizing the Josephson energy

$$E = -\cos\phi_{s1} - J_{s2}\cos\phi_{s2} - J_{12}\cos(\phi_{s1} - \phi_{s2}), \quad (32)$$

which yields

$$\sin\phi_{s1} + J_{s2}\sin\phi_{s2} = 0, \qquad (33)$$

$$\sin\phi_{s1} + J_{12}\sin(\phi_{s1} - \phi_{s2}) = 0. \qquad (34)$$

We see that if $\hat{\phi} = (\phi_{s1}, \phi_{s2})$ is a solution, then $\hat{\phi}_2 = -\hat{\phi} = (-\phi_{s1}, -\phi_{s2})$ is also a solution. If these two solutions are distinct, which means that one can not obtain $\hat{\phi}_2$ from $\hat{\phi}$ by changing the phases by $2n\pi$ with an integer n, then TRS is broken in the junction.

In one TRSB state (ϕ_{s1}, ϕ_{s2}), the interjunction Josephson current flows from the second band in the two-band superconductor to the s-wave superconductor, and then flows back to
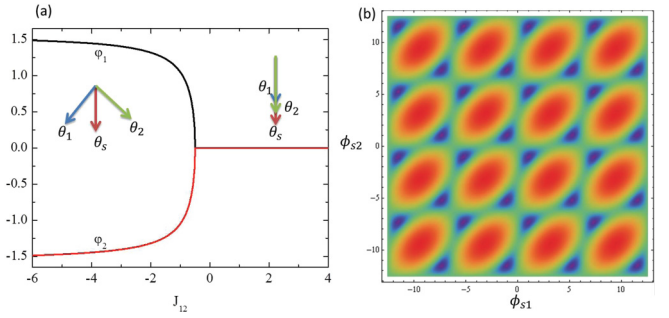

FIG. 2. (Color online) (a) Phase diagram of Josephson junctions with $s\pm$ pairing symmetry. Here, $J_{s2} = J_{s1} = 1$. For $J_{12} < -0.5$, TRSB occurs and the transition is continuous. There are two degenerate ground states $\hat{\phi} = (\phi_{s1}, \phi_{s2})$ and $-\hat{\phi}$. Only one configuration of phases in the ground state with TRSB is shown in the figure. (b) Energy landscape in the TRSB state with $J_{12} = -1$ and $J_{s2} = 1$. There are many degenerate and separated energy minima (blue region), $\hat{\phi}$, $-\hat{\phi}$ and other minima obtained by shifting phases by $2n\pi$ with an integer n. To contrast the minima, we plot $\ln(E + 1.6)$.

the first band in the two-band superconductor. The net current is finally balanced by the interband Josephson current from the first band to the second band in the two-band superconductor. In the other TRSB state $(-\phi_{s1}, -\phi_{s2})$, the supercurrent flow reverses direction. The meaning of TRSB becomes explicit in this picture. Please note that the supercurrent loop flows in the band space, thus is not coupled with the gauge field. No spontaneous magnetic flux is induced for spatially homogeneous systems. However, as will be demonstrated in the following, in the ground state with TRSB, spontaneous magnetic flux will be induced when the Josephson coupling is perturbed locally.

For $J_{12} > 0$, the ground state is trivial $\phi_{s1} = \phi_{s2} = 0$. However, for $J_{12} < 0$, nontrivial solution for ϕ_{si} occurs due to the frustrated interaction. Let us consider $J_{12} < 0$ and $|J_{12}| \gg J_{si}$. In this case, $\phi_{s1} = \phi_{s2} + \pi + \delta$ with $\delta \ll 1$. We then expand Eqs. (33) and (34) in terms of δ, and obtain

$$\cos\phi_{s2} = (1 - J_{s2})J_{12}/J_{s2}, \qquad (35)$$

when $J_{12} > -|J_{s2}/(1 - J_{s2})|$. Otherwise, $\phi_{s2} = 0$ if $J_{s2} > J_{s1}$ and $\phi_{s2} = \pi$ if $J_{s2} < J_{s1}$. Thus, TRSB occurs at $J_{12} = -|J_{s2}/(1 - J_{s2})|$. The condition $J_{12} \gg J_{si}$ is satisfied when J_{s1} and J_{s2} are comparable. This is reasonable since frustration is maximized when $J_{s1} \sim J_{s2}$.

For a symmetric coupling $J_{s2} = J_{s1} = 1$, we have $\phi_{s1} = -\phi_{s2}$ and the ground state can be found exactly. For $J_{12} > -0.5$, we have TRS state with $\phi_{s1} = \phi_{s2} = 0$. For $J_{12} \leqslant -0.5$, TRSB occurs with $\cos\phi_{s1} = -1/(2J_{12})$. A typical phase diagram and the the energy landscape are shown in Fig. 2.

V. CRITICAL CURRENT

In this section, we calculate the dependence of the critical current on the applied magnetic fields. Because of the interference between two tunneling channels $J_{s1}\sin\phi_{s1}$ and $J_{s2}\sin\phi_{s2}$, the critical current of the junction depends on

the phase difference between two tunneling channels. We consider a short junction L where the screening current can be neglected. [Precisely, L should be much smaller than the longer length in Eqs. (47) and (48)]. The presence of magnetic field induces a spatial variation of phases. Without the screening effect, the phase can be written as

$$\phi_{s1} = \phi_{s10} + k_B x + \phi_I \quad \text{and} \quad \phi_{s2} = \phi_{s20} + k_B x + \phi_I, \tag{36}$$

where $k_B = C_b B_a/(\zeta_1^{-1} + \zeta_2^{-1})$ is the phase gradient created by the applied field according to the boundary condition (31), ϕ_I is the phase created by external current, and ϕ_{si0} is the phase in the ground state. We have neglected the magnetic field induced by the external current because it is weak compared to B_a. The critical current I is then expressed as

$$
\begin{aligned}
\frac{I}{L} &= \frac{1}{L} \int_0^L (\sin \phi_{s1} + J_{s2} \sin \phi_{s2}) dx \\
&= \left| \frac{\sin \Phi}{\Phi} [\cos \phi_{s10} + J_{s2} \cos \phi_{s20}] \right|,
\end{aligned}
\tag{37}
$$

where we have used the ground-state conditions (33) and (34), and $\Phi \equiv k_B L/2$. Aside from the conventional factor responsible for the Fraunhofer pattern, we have an additional term accounting for the interference between different tunneling channels. When $J_{12} > 0$ for $s++$ superconductors, the two channels add constructively, while for $s\pm$ superconductors with $-J_{12} \gg J_{si}$, we have $\phi_{s1} \approx \pi + \phi_{s2}$, and the two channels cancel destructively. The TRSB state with finite $0 < \phi_{si0} < \pi$ interpolates these two limiting cases. We also note that the two different TRSB states $\hat{\phi}$ and $-\hat{\phi}$ have the same critical current. The dependence of critical current on magnetic field is depicted in Fig. 3 for three different cases.
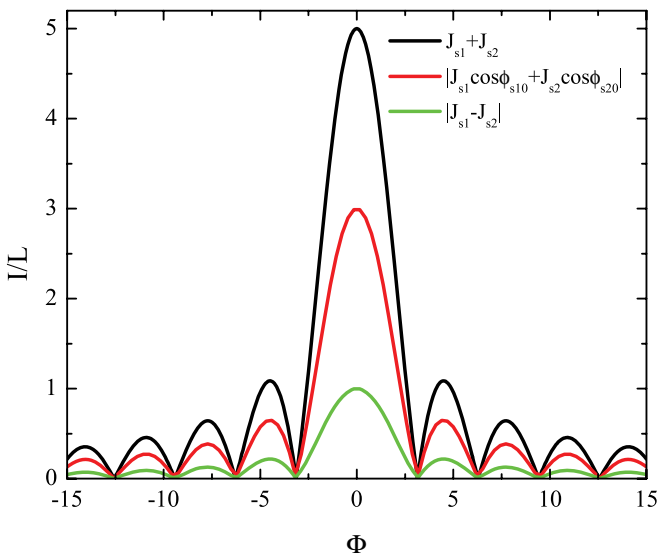

FIG. 3. (Color online) Dependence of critical current on magnetic fields in three different regimes: $J_{12} > 0$ with $\phi_{s1} = \phi_{s2}$, $-J_{12} \gg J_{si}$ with $\phi_{s1} = \phi_{s2} + \pi$, and the TRSB state.

VI. SHAPIRO STEPS

In this section, we investigate the response of the junction to external microwave irradiation. When the external irradiation is locked with the internal plasma oscillation, current steps are induced known as the Shapiro steps.[47] In the presence of incident waves with frequency ω, the voltage across the junction can be written as $E = E_{\rm dc} + \tilde{E} \sin(\omega t)$. According to the generalized ac Josephson relation, the gauge-invariant phase differences can be written as

$$\phi_{s1} = \phi_{s10} + \omega_0 t + A \sin(\omega t) + \phi_I, \tag{38}$$

$$\phi_{s2} = \phi_{s20} + \omega_0 t + A \sin(\omega t) + \phi_I, \tag{39}$$

with $\omega_0 = C_e(\alpha_1^{-1} + \alpha_2^{-1})^{-1} E_{\rm dc}$ and $A = C_e(\alpha_1^{-1} + \alpha_2^{-1})^{-1} \tilde{E}/\omega$, and ϕ_I an arbitrarily relative phase between the Josephson oscillation and incident wave. Experimentally, when one fixes the voltage and tunes the current, ϕ_I will adjust correspondingly. The Josephson current then is given by

$$
\begin{aligned}
I &= \langle (\sin \phi_{s1} + J_{s2} \sin \phi_{s2}) \rangle_t = \sum_n \{\cos(\phi_{s10}) \\
&\quad + J_{s2} \cos(\phi_{s20})\} J_n(A) \sin[(\omega_0 - n\omega)t + \phi_I], \tag{40}
\end{aligned}
$$

where J_n is the Bessel function of the first kind and we have again used the ground-state conditions (33) and (34). $\langle \ldots \rangle_t$ denotes time average. When the resonance condition

$$C_e \left(\alpha_1^{-1} + \alpha_2^{-1} \right)^{-1} E_{\rm dc} = n\omega \tag{41}$$

is satisfied, the Shapiro steps appear with the height

$$I_s = 2 \left| [\cos(\phi_{s10}) + J_{s2} \cos(\phi_{s20})] J_n(A) \right|. \tag{42}$$

Again, the height of the Shapiro steps depends on the relative phase of the different channels, similar to that in the critical current in Eq. (37).

VII. JOSEPHSON PLASMA MODE

The low-energy collective oscillation in a Josephson junction is called Josephson plasma, which is composite waves of electromagnetic fields and Josephson current. It determines lower-energy physical properties and transport properties of the junction, such as the Fiske and Eck resonances.[48] Moreover, the dispersion for the plasma modes can be measured by Josephson plasma resonance,[49] which provides a useful tool to extract physical parameters of the junction. In this section, we calculate the dispersion of the Josephson plasma in the heterotic junction between a multiband superconductor and a single-band superconductor.

For convenience of calculations, we take $\alpha_s = \alpha_1 = \alpha_2 = \alpha \ll 1$, $\zeta_s = \zeta_1 = \zeta_2 = \zeta$, and $J_{s1} = J_{s2} = 1$. We expand the phases around their ground state value $\bar{\phi}_{si}$, $\phi_{si} = \bar{\phi}_{si} + \varphi_{si}$, with $\bar{\phi}_{s2} = -\bar{\phi}_{s1} = \phi_0$. We then take the Fourier transform of φ_{si}, $\varphi_{si}(x,t) \sim \varphi_{si}(k,\omega) \exp[i(kx - \omega t)]$. Substituting into

Eqs. (22) and (26), we have the following equations:

$$\left(\frac{-k^2}{3\zeta + 2} + \frac{\omega^2}{2} - \cos\phi_0\right)(\varphi_{s1} + \varphi_{s2}) = 0, \qquad (43)$$

$$\left(\frac{-1}{2\epsilon_b\alpha}\omega^2 + \frac{k^2}{\zeta}\frac{3\zeta + 1}{3\zeta + 2} + 2\cos\phi_0 + J_{12}\cos(2\phi_0)\right)\varphi_{s1}$$
$$+ \left(\frac{1}{2\epsilon_b\alpha}\omega^2 - \frac{k^2}{\zeta}\frac{1}{3\zeta + 2} + \cos\phi_0 - J_{12}\cos(2\phi_0)\right)$$
$$\times \varphi_{s2} = 0. \qquad (44)$$

We then derive two branches of the dispersion relation

$$\omega_1^2 = 2\cos\theta_0 + \frac{2k^2}{3\zeta + 2}, \qquad (45)$$

$$\omega_2^2 = \epsilon_b\alpha\left[\frac{k^2}{\zeta} + \cos\phi_0 + 2J_{12}\cos(2\phi_0)\right], \qquad (46)$$

with $\cos\phi_0 = -1/(2J_{12})$. The results are displayed in Fig. 4. There are two Swihart velocities with $c_1 = \sqrt{2/(3 + 2\zeta)}$ and $c_2 = \sqrt{\epsilon_b\alpha/\zeta}$. The splitting of the Josephson plasma into two branches thus supports Cherenkov radiation in the junction, similar to that in a stack of Josephson junctions.[50,51] In the TRSB state, the plasma modes for the two degenerate TRSB pair states $\hat{\phi}$ and $-\hat{\phi}$ are identical. The mode ω_1 corresponds to the in-phase oscillation of φ_{s1} and φ_{s2}, and is always massive. The mode ω_2 corresponds to the out-of-phase oscillation, which is similar to the Leggett mode[52] in bulk multiband superconductors. In the limit of $\alpha \to 0$, this mode disappears because the out-of-phase oscillation is forbidden according to the ac Josephson relation $\partial_t\phi_{s1} = \partial_t\phi_{s2} = E_{b,z}$. In the presence of charge neutrality breaking, the mode ω_2 becomes massless at the TRSB transition $\cos\phi_0 + 2J_{12}\cos(2\phi_0) = 0$. Close to the TRSB transition, the angle between ϕ_{s1} and ϕ_{s2} is about to grow continuously from 0 to a finite value as shown in Fig. 2(a), thus the out-of-phase oscillation becomes a soft mode.

Near a continuous phase transition, the energy cost for the excitation of perturbations is close to zero, thus can be easily
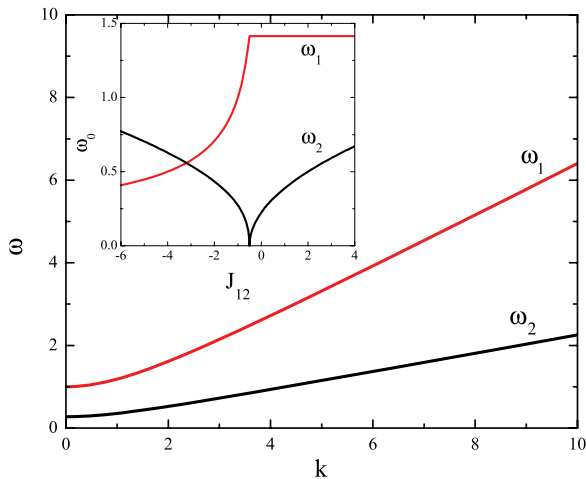

FIG. 4. (Color online) Dispersion of two Josephson plasma modes according to Eqs. (45) and (46). We use $\zeta = 1$, $\alpha = 0.05$, and $\epsilon_b = 1$ in the plot. Inset is the energy gap $\omega_1(k = 0)$ and $\omega_2(k = 0)$ as a function of J_{12}. The branch $\omega_2(k)$ becomes massless at the TRSB transition.

excited, which in turn tends to destroy the ordered state. At the second-order TRSB transition, the out-of-phase oscillations ϕ_{s1} and ϕ_{s2} do not cost energy and the phase rigidity for the out-of-phase oscillation vanishes. (The phase rigidity for the in-phase oscillation is nonzero, see Fig. 4.) In bulk superconductors, this phase rigidity is proportional to the superfluid density and the mass of photon according to the Anderson-Higgs mechanism.[38] The vanishing of the phase rigidity in the junction means that the photon mass becomes zero.

The massless plasma mode at the TRSB transition in Eq. (46) is remarkable. In a conventional Josephson junction where the superconductivity is suppressed in the barrier, the mass of the Josephson plasma is reduced compared to that in bulk, but the plasma excitation still has an energy gap proportional to the Josephson coupling. Here, we show that there exists genuine massless photon in a junction with TRSB. The massless plasma mode is analogous to the massless Leggett boson discussed in bulk superconductors with TRSB.[53] The difference is that the Leggett mode is a purely phase mode, while the plasma mode is a composite mode of superconducting phase and gauge fields. The massless Josephson plasma mode gives rise to phenomena as will be elucidated in the next section.

VIII. JOSEPHSON PENETRATION DEPTH AND H_{c1}

In this section, we calculate the Josephson penetration depth and the threshold magnetic field H_{c1} where magnetic flux starts to penetrate into the junctions.[54] The penetration depth is determined by the mass of the photon in the junction according to the London equation. By setting $\omega = 0$ in Eqs. (45) and (46), we obtain the Josephson penetration depth

$$\lambda_{J1} = 1/\sqrt{(3\zeta + 2)\cos\phi_0}, \qquad (47)$$

$$\lambda_{J2} = 1/\sqrt{\zeta\left[\cos\phi_0 + 2J_{12}\cos(2\phi_0)\right]}. \qquad (48)$$

The Josephson penetration depth of the junction is given by the larger value of λ_{J1} and λ_{J2}. Being a static property, the Josephson penetration depth is independent of α. At the TRSB transition, λ_{J2} diverges as a consequence of the vanishing photon mass.

In conventional type-II superconductors, magnetic fields can penetrate into the superconductor only when they are larger than a critical value H_{c1}, due to the screening of fields as a consequence of massive photons. This becomes evident when we look at $H_{c1} \sim \Phi_0/\lambda_L^2$ obtained under the London approximation. Here, the London penetration depth λ_L is inverse proportional to the mass of photon $\lambda_L \sim 1/\sqrt{m_p}$. For a conventional Josephson junction, H_{c1} is reduced as a result of weakened superconductivity in the junction, but H_{c1} is nonzero $H_{c1} > 0$. In junctions with massless photons at TRSB transition, the magnetic field can penetrate easily into the system, and the lower critical field becomes zero, $H_{c1} = 0$.

IX. MCCUMBER SOLUTION

In the absence of applied magnetic fields, the phases are uniform along the x direction for a homogeneous junction. When the external current exceeds the critical current I_c of the junction Eq. (36), the junction switches into a resistive state and

the phases start to rotate; such a state is called the McCumber state.[55] For an overdamped junction [β_d in Eq. (28) is large $\beta_d \gg 1$; the standard McCumber number is given by $1/\beta_d^2$], the junction returns to zero-voltage state when the external current is smaller than I_c. However, for an underdamped junction with $\beta_d \ll 1$, the system remains resistive, until a current much smaller than I_c where the system transits into zero-voltage state again.[56] In this section, we calculate the *IV* curve in the McCumber state.

The phases in the McCumber state, for a symmetric coupling $J_{s2} = J_{s1}$, can be written as

$$\phi_{s1} = \phi_0 + \omega t + \text{Re}[-i\varphi_{s1} \exp(i\omega t)], \tag{49}$$

$$\phi_{s2} = -\phi_0 + \omega t + \text{Re}[-i\varphi_{s2} \exp(i\omega t)]. \tag{50}$$

Substituting Eqs. (49) and (50) into Eqs. (22) and (26) and approximating $\sin(\phi_{s1}) \approx -i \exp[i(\phi_0 + \omega t)]$, we have

$$\left[\frac{-\omega^2}{2\epsilon_b\alpha} + J_{12}\cos(2\phi_0)\right]\varphi_{s1} + \left[\frac{\omega^2}{2\epsilon_b\alpha} - J_{12}\cos(2\phi_0)\right]\varphi_{s2}$$
$$= -[2\exp(i\phi_0) + \exp(-i\phi_0)], \tag{51}$$

$$\omega^2 (\varphi_{s1} + \varphi_{s2}) = 4\cos(\phi_0). \tag{52}$$

Equations (51) and (52) can be solved and we have

$$\varphi_{s1} = \frac{2\cos\phi_0}{\omega^2} + \frac{2\exp(i\phi_0) + \exp(-i\phi_0)}{\omega^2/(\epsilon_b\alpha) - 2J_{12}\cos(2\phi_0)}, \tag{53}$$

$$\varphi_{s2} = \frac{2\cos\phi_0}{\omega^2} - \frac{2\exp(i\phi_0) + \exp(-i\phi_0)}{\omega^2/(\epsilon_b\alpha) - 2J_{12}\cos(2\phi_0)}. \tag{54}$$

Then, the supercurrent contributed from the phase oscillation is given by

$$J_s = \langle\sin(\phi_{s1}) + J_{s2}\sin(\phi_{s2})\rangle_t$$
$$= -\text{Re}\left[\sin\phi_0 \frac{2\exp(i\phi_0) + \exp(-i\phi_0)}{\omega^2/(\epsilon_b\alpha) - 2J_{12}\cos(2\phi_0)}\right]. \tag{55}$$

The supercurrent increases when voltage ω decreases. The total current density is $J = \beta_d\omega + J_s$, with an Ohmic contribution $\beta_d\omega$.

X. FLUX-FLOW REGION: FISKE AND ECK RESONANCES

When strong magnetic fields are applied parallel to the junction, magnetic fields penetrate into the junction and form Josephson vortices. Under a transport current, the vortices are driven by the Lorentz force and move along the junction, which induces finite voltage across the junction. Then, the Josephson plasma is excited. When the plasma is resonant with the vortex motion, it induces a large dc part of supercurrent, which manifests as a current step known as the Eck step.[57] For a junction of finite length, the plasma can be resonant with the cavity formed by the junction itself under appropriate conditions, which also induces current steps known as the Fiske steps.[58] In this section, we calculate the resonances in the flux-flow region. Studies of the flux-flow dynamics in two-band junctions with an emphasis on the interband Josephson coupling were presented in Ref. 59 very recently.

For a junction with a finite length L and with a symmetric coupling $J_{s2} = J_{s1}$, the phase in the flux-flow region can be written as

$$\phi_{s1} = \phi_0 + k_B x + \omega t + \text{Re}[-i\varphi_{s1}\cos(k_m x)\exp(i\omega t)], \tag{56}$$

$$\phi_{s2} = -\phi_0 + k_B x + \omega t + \text{Re}[-i\varphi_{s2}\cos(k_m x)\exp(i\omega t)], \tag{57}$$

where $k_B = C_b B_a / (\zeta_1^{-1} + \zeta_2^{-1})$ is the phase gradient due to the applied field B_a. Here, $k_m = m\pi/L$ accounts for the geometric resonances, and ϕ_0 is the ground-state value. By substituting Eqs. (56) and (57) into Eqs. (22) and (26) and using $\sin(\phi_{s1}) \approx -i\exp[i(\phi_0 + k_B x + \omega t)]$ to the zeroth order, we have

$$\left[\frac{\omega^2}{2\epsilon_b\alpha} - J_{12}\cos(2\phi_0)\right](\varphi_{s2} - \varphi_{s1}) + \frac{k_m^2}{\zeta}\frac{3\zeta + 1}{3\zeta + 2}\varphi_{s1}$$
$$- \frac{k_m^2}{\zeta}\frac{1}{3\zeta + 2}\varphi_{s2} = -[2\exp(i\phi_0) + \exp(-i\phi_0)]F_c, \tag{58}$$

$$\left(\frac{-k_m^2}{3\zeta + 2} + \frac{\omega^2}{2}\right)(\varphi_{s1} + \varphi_{s2}) = 2\cos(\phi_0)F_c, \tag{59}$$

where we have introduced the coupling between the flux flow and plasma oscillation at the cavity modes k_m:

$$F_c = \frac{2}{L}\int_0^L dx \cos(k_m x)\exp(ik_B x). \tag{60}$$

Resonances occur at

$$\omega^2 = \frac{2k_m^2}{3\zeta + 2}, \tag{61}$$

$$\frac{1}{\epsilon_b\alpha}\omega^2 = \frac{k_m^2}{\zeta} + 2J_{12}\cos(2\phi_0), \tag{62}$$

that is, when the plasma frequency matches the cavity frequency. Thus, in the presence of the charge neutrality breaking, there are two resonant peaks for a given cavity mode m because there are two different dispersion branches. The supercurrent induced by the resonance is

$$J_s = \frac{1}{L}\int \langle\sin(\phi_{s1}) + J_{s2}\sin(\phi_{s2})\rangle_t \, dx$$
$$= \frac{-iF_c^*}{4}\left[\varphi_{s1}\exp(-i\phi_0) + J_{s2}\varphi_{s2}\exp(i\phi_0)\right], \tag{63}$$

where again the terms in the square brackets account for the interference between two tunneling channels. Real junction inevitably involves dissipation, and the delta-peak resonance in Eqs. (61) and (62) is rounded by the dissipation. A formal treatment would introduce dissipation function as discussed in Eq. (28). Here, we introduce phenomenologically the dissipation by the replacement $\omega^2 \leftarrow \omega^2 - i\beta_d\omega$. We calculate the *IV* curve by solving Eqs. (58)–(60) and (63) numerically and the result is displayed in Fig. 5(a), where two resonant peaks can be clearly observed.

For a long junction, the geometry resonance is not important. In this case, we need to replace the solutions in Eqs. (56) and (57) by $k_m \leftarrow k_B$, i.e., the plasma has the same spatial modulation as the flux flow along the x direction because the plasma oscillation is excited by the flux flow. The expressions of the resonance conditions and *IV* curves are the same as those of the Fiske resonance except for the replacement of $k_m \leftarrow k_B$. When the velocity of the flux flow matches the
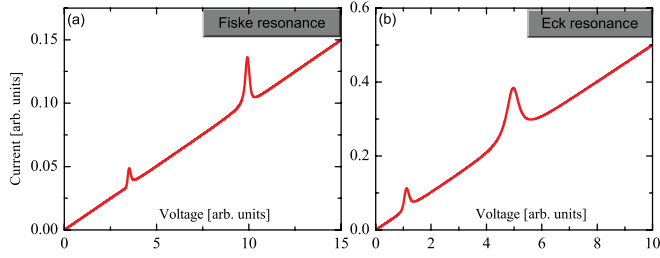
FIG. 5. (Color online) (a) *IV* curve in the flux-flow region. The resonance peaks shown in the figure are caused by the excitation of cavity modes (Fiske resonance). Here, we only plot the resonance mode $k_m = \pi/L$ with $L = 0.2$. We use $\zeta = 1$, $\alpha = 0.05$, $\epsilon_b = 1$, and $B_a = \pi$. The Ohmic contribution in the figure is $\beta_d \omega$ with $\beta_d = 0.01$. (b) Eck resonance in the flux-flow region. We use $\zeta = 1$, $\alpha = 0.05$, $\epsilon_b = 1$, $B_a = \pi$, and $\beta_d = 0.05$.

velocity of plasma (there are two dispersion relations with two different velocities), current steps known as Eck steps appear as shown in Fig. 5(b).

For a stack of conventional Josephson junctions, the plasma dispersion splits into N branches with N the number of junctions.[60–62] It gives N resonant branches in the *IV* characteristic for a given mode. The experimental observation of N resonant branches thus confirms the plasma splitting in junction stacks.[63] Similarly, the charge neutrality breaking effect discussed here can also be checked experimentally by measurement of doubling of resonant branches in the *IV* characteristic.

XI. TOPOLOGICAL EXCITATIONS

In the present system, the potential energy has many degenerate minima, which differ in ϕ_{si} by 2π, as shown in Eq. (32) and Fig. 2(b). In the TRSB state, there are additional minima at $\hat{\phi}$ and $-\hat{\phi}$ due to TRSB. Thus, the system supports stable topological excitations, categorized as solitons or phase kinks belonging to the homotopy class of $\pi_0(S^0)$.[64] There are solitons with two different types of origins, with one being the soliton between the energy minima with $2n\pi$ phase shift, and the other the soliton between two TRSB pair states $\hat{\phi}$ and $-\hat{\phi}$. The width of the phase kink is determined by the optimization between the potential energy in Eq. (32) and the energy due to the phase gradient. When the width of kink increases, the cost in the potential energy increases while the cost in energy associated with the phase gradient decreases, and vice versa. The stable kink solution compromises these two energy costs. In this section, we investigate the possible soliton solutions in the junction. For discussions of phase kink in bulk multiband superconductors, please see Refs. 65–67.

First, let us consider the soliton solution by changing ϕ_{si} by $2n_i\pi$ with an integer n_i. The total magnetic flux associated with these solitons is given by

$$\Phi(n_i) = \left(\zeta_1^{-1} 2n_i\pi + \zeta_2^{-1} 2n_2\pi \right) / C_b. \tag{64}$$

It is fractional quantized if $n_1 \neq n_2$. Unlike the fractional quantized vortices in bulk multiband superconductors,[68] the energy associated with the fractional soliton in junctions is bounded, thus the excitation is thermodynamically stable. We calculate numerically a typical configuration of the soliton in the junction, where ϕ_{s1} changes by 2π and ϕ_{s2} does not change

from the left edge to the right edge. The results are shown in Fig. 6(a). The presence of solitons breaks TRS, even though in the ground state, the system has TRS.

Now, let us investigate the soliton solution between two TRSB pair states $\hat{\phi}$ and $-\hat{\phi}$, when the ground breaks TRS. An exact expression can be found for the symmetric case $\zeta_s = \zeta_1 = \zeta_2 = \zeta$ and $J_{s1} = J_{s2} = 1$. In this case, $\phi_{s1}(x) = -\phi_{s2}(x)$, and the equation for the spatial variation of phase becomes

$$-\frac{1}{\zeta}\partial_x^2\phi_{s1} + \sin\phi_{s1} + J_{12}\sin(2\phi_{s1}) = 0. \tag{65}$$

We use the Bogomolny method[64] to find the exact solution in the following. The energy corresponding to Eq. (65) is

$$E_s = \frac{(\partial_x\phi_{s1})^2}{2\zeta} - (\cos\phi_{s1} - \cos\phi_0)$$
$$- \frac{J_{12}}{2}[\cos(2\phi_{s1}) - \cos(2\phi_0)], \tag{66}$$

where $\cos\phi_0 = -1/(2J_{12})$ is the ground-state value and we introduce them into E_s to shift the energy minimum to 0. We then consider the following inequality:

$$\left(\frac{1}{\sqrt{2\zeta}}\partial_x\phi_{s1} \pm \sqrt{U} \right)^2 \geqslant 0, \tag{67}$$

with $U = (\sqrt{-J_{12}}\cos\phi_{s1} - \frac{1}{2\sqrt{-J_{12}}})^2$. Thus, the energy of the kink has a lower bound

$$E_s = \frac{1}{2\zeta}(\partial_x\phi_{s1})^2 + U \geqslant \pm \frac{\sqrt{2}}{\sqrt{\zeta}}\partial_x\phi_{s1}\sqrt{U}. \tag{68}$$

The lower bound is reached when

$$\partial_x\phi_{s1} = \pm\sqrt{2\zeta U} = \pm\sqrt{2\zeta}\left(\sqrt{-J_{12}}\cos\phi_{s1} - \frac{1}{2\sqrt{-J_{12}}} \right). \tag{69}$$

Equation (69) can be integrated explicitly, which yields a soliton solution between the two TRSB pair states

$$\phi_{s1} = 2\tan^{-1}\left[\frac{\sqrt{-1+4J_{12}^2}}{1-2J_{12}}\tanh\left(\pm\frac{\sqrt{\zeta}\sqrt{-1+4J_{12}^2}}{2\sqrt{2}\sqrt{-J_{12}}}x \right) \right], \tag{70}$$

where "plus" corresponds to soliton and "minus" corresponds to antisoliton. The energy associated with the kink is

$$E_s = \sqrt{\frac{2}{\zeta}}\left| \left(2\sqrt{-J_{12}}\sin\phi_0 - \frac{1}{\sqrt{-J_{12}}}\phi_0 \right) \right|. \tag{71}$$

In the symmetric case as we studied here, there is no magnetic flux associated with the soliton because the phase gradient in each channel compensates exactly $\partial_x(\phi_{s1} + \phi_{s2}) = 0$. However, for more general cases, the soliton carries finite magnetic flux. We calculate numerically the soliton solution and the associated magnetic flux for asymmetric parameters $\zeta_1 \neq \zeta_2 \neq \zeta_s$, and the results are displayed in Fig. 6(b). Suppose at the left domain, the phases belong to one ground state $-\phi_{s10}$ and $-\phi_{s20}$, and at the right domain, the phases
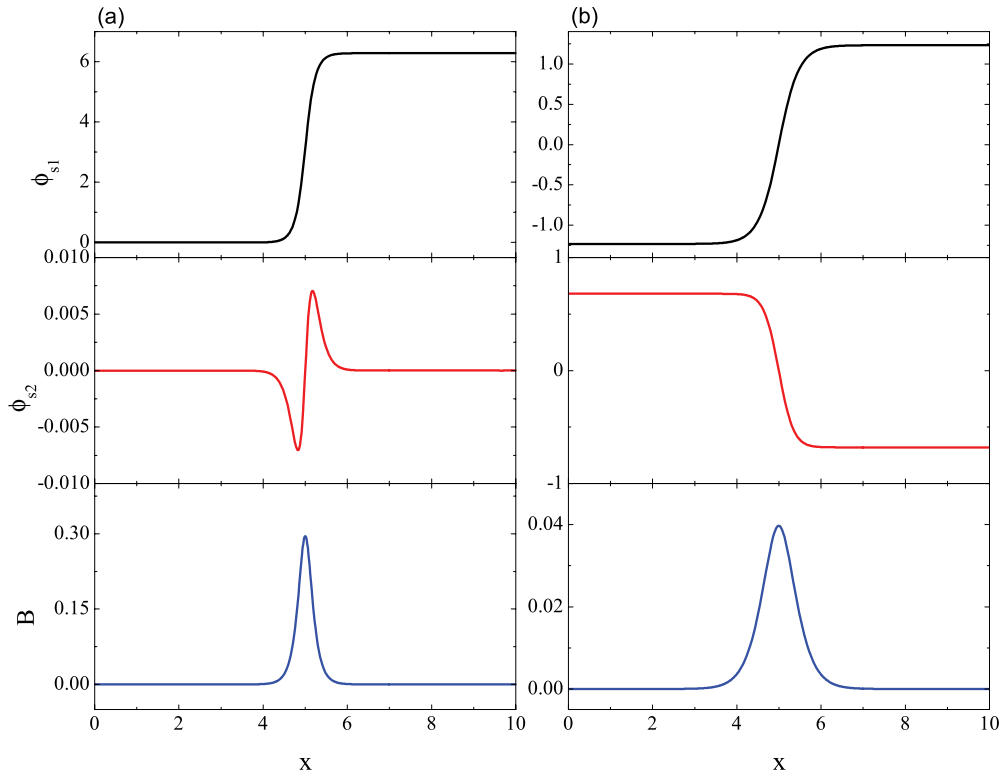
FIG. 6. (Color online) (a) Profile of phases and magnetic field in (a) a conventional 2π soliton, where ϕ_{s1} changes by 2π, (b) soliton between two TRSB pair states. Here, $\zeta_1 = 10$, $\zeta_2 = 24$, $\zeta_s = 20$, $J_{s1} = 1.0$, $J_{s2} = 1.5$. $J_{12} = 1.0$ in (a) and $J_{12} = -1.0$ in (b).

belong to the other ground state ϕ_{s10} and ϕ_{s20}, the total magnetic flux is quantized in terms of ϕ_{si0}:

$$\Phi = 2\left(\zeta_1^{-1}\phi_{s10} + \zeta_2^{-1}\phi_{s20}\right)/C_b. \tag{72}$$

The discussions of the solitons so far are restricted to the static case where the stability of solitons is guaranteed by the energy landscape of the Josephson coupling. In the dynamic region when a transport current is present, solitons can be stabilized with some voltages. Solitons can also be created due to the dynamic instability of superconducting phase in the Josephson junctions.[69] The solitons start to move because of the Lorentz force. When the velocity of soliton matches the velocity of plasma, current steps known as the zero-field steps arise at these voltages.[70] Due to the existence of various types of fractionally quantized solitons and the existence of two Swihart velocities for plasma in the present system, we expect appearance of many zero-field steps in the *IV* curve.

The existence of solitons associated with flux in Eq. (64) does not depend on the pairing symmetry of the two-band superconductors, while the soliton between two TRSB pair states in Eq. (70) exists only in superconductors with $s\pm$ pairing symmetry, where TRSB in the ground state is possible.

XII. SPONTANEOUS MAGNETIC FLUX

In this section, we investigate the spontaneous magnetic flux in junctions unique to superconducting electrodes with the $s\pm$ pairing symmetry, which points to a practically useful way to detect the pairing symmetry. We consider a junction with spatial variation of the Josephson couplings, which is likely

realized in real systems due to inhomogeneity, such as variation of the thickness of barrier, or can be tuned intentionally as in Ref. 24. Let us first consider a step modulation of the Josephson coupling, which is amenable to analytical calculation

$$J_{s2} - J_{s1} = J'[2\Theta(x) - 1], \tag{73}$$

with the Heaviside step function $\Theta(x)$. We further assume $-J_{12} \gg J_{si}$, and the spatial variation of phase is given by, according to Eq. (27),

$$\lambda_e^2 \partial_x^2 \phi_{s1} - J'[-2\Theta(x) + 1]\sin\phi_{s1} = 0, \tag{74}$$

with the boundary condition $\partial_x\phi_{s1}(x = \pm L/2) = 0$. The length of the junction L is assumed to be small $L \ll \lambda_e$. In this case, the solution can be expressed as

$$\phi_{s1}(x) = \phi_{s10} + \eta(x)\sin\phi_{s10}, \tag{75}$$

with $\eta(x) \ll 1$. By substituting the solution into Eq. (74), we obtain the equation for $\eta(x)$:

$$\lambda_e^2 \partial_x^2 \eta(x) - J'[-2\Theta(x) + 1][1 + \eta(x)\cos\phi_{s10}] = 0. \tag{76}$$

The first term in the second square brackets dominates and to the first order, we can safely neglect the second term in the square brackets. Integrating along the x direction yields the magnetic flux

$$B = \frac{\zeta_1^{-1} + \zeta_2^{-1}}{C_b}\sin\phi_{s10}\partial_x\eta(x) = J'\sin\phi_{s10}\left(-\frac{L}{2} + |x|\right). \tag{77}$$

ϕ_{s10} is given by the condition that spatial average of Eq. (76) vanishes because of the boundary condition $\partial_x\phi_{s1} = 0$ as no

external magnetic field is applied:

$$\int_{-L/2}^{L/2} J'[-2\Theta(x) + 1]\eta(x)\cos\phi_{s10}dx = 0, \quad (78)$$

which yields $\phi_{s10} = \pi/2$.

The magnetic flux inside depends on the length of junction and is not quantized for a short junction $L \ll \lambda_e$. However, for a long junction $L \gg \lambda_e$, magnetic flux only occurs in the region where the Josephson coupling changes and it is quantized due to the complete screening. We investigate the magnetic flux in a long junction $L \gg \lambda_e$, where the nonlinear effect of Josephson current must be treated self-consistently. The solution can be constructed as follows: for $x < 0$,

$$\phi_{s1}^L = 4\arctan\left[\exp\left(\frac{\sqrt{J'}}{\lambda_e}(x + x_0)\right)\right], \quad (79)$$

and for $x > 0$,

$$\phi_{s1}^R = 4\arctan\left[\exp\left(\frac{\sqrt{J'}}{\lambda_e}(x - x_0)\right)\right] - \pi. \quad (80)$$

At $x = 0$, the derivative of ϕ_{s1} is automatically continuous under this construction. x_0 is determined by the continuity condition $\phi_{s1}^L(x = 0) = \phi_{s1}^R(x = 0)$, which yields $x_0 = \lambda_e \ln(-1 + \sqrt{2})/\sqrt{J'}$. The total magnetic flux inside the junction is given by

$$\Phi = \int_{-L/2}^{L/2} B\,dx = \frac{\zeta_1^{-1} + \zeta_2^{-1}}{C_b}\int_0^\pi \partial_x\phi_{s1} = \frac{\zeta_1^{-1} + \zeta_2^{-1}}{C_b}\pi, \quad (81)$$

and is quantized since ϕ_{s1} run from 0 at $x = -L/2$ to π at $x = L/2$. The profiles of phases and magnetic field are shown in Fig. 7.

The modulation of the Josephson coupling Eq. (73) can be simplified into a setup shown in Fig. 8(a), where a loop made of conventional s-wave superconductor is in contact with a two-band superconductor and forms two point junctions. This geometry is the same as the one studied experimentally in Ref. 29.
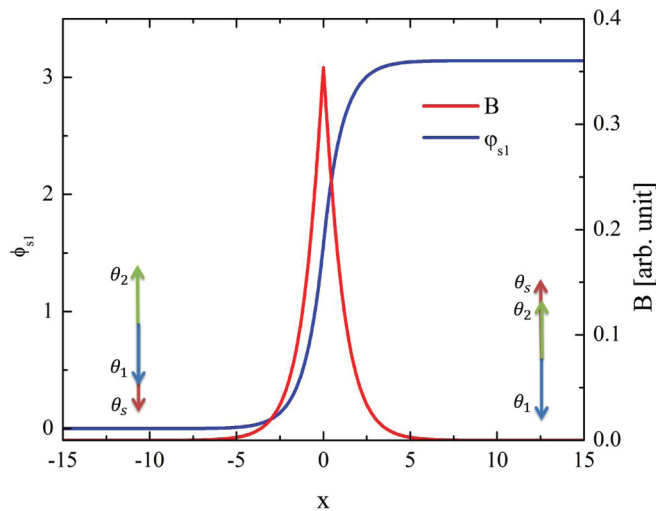

FIG. 7. (Color online) Profile of the phases and magnetic field with a step modulation of the Josephson coupling in a junction with $s\pm$ pairing symmetry. Here, $\phi_{s2} = \phi_{s1} + \pi$ and $\lambda_e = J' = 1$.
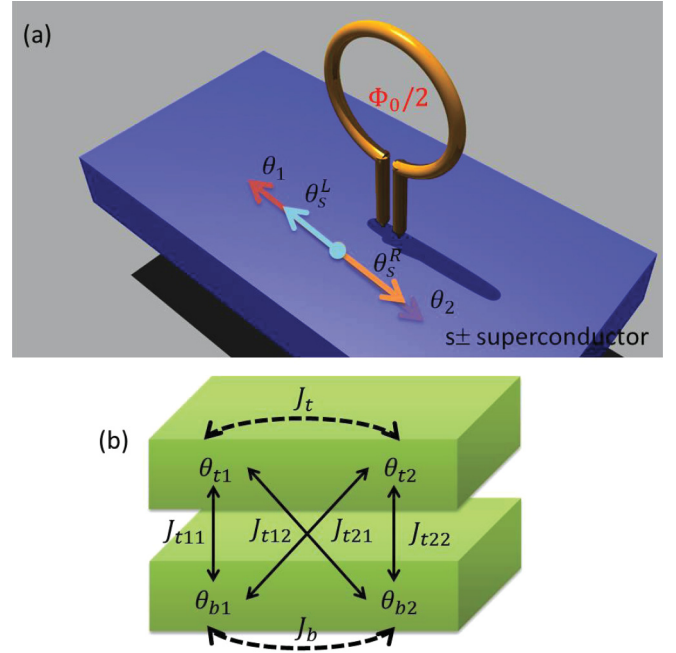

FIG. 8. (Color online) (a) Experimental proposal to detect the pairing symmetry in multiband superconductors. (b) Grain-boundary Josephson junctions in multiband superconductors.

When $|J_{12}| \gg J_{si}, \theta_1 = \pi + \theta_2$. If at the left contact $J_{s1} > J_{s2}$, then $\theta_s^L = \theta_1$. However, if one can achieve at the right end $J_{s2} < J_{s1}$, then $\theta_s^R = \theta_2 = \theta_1 + \pi$ when the self-inductance is small for a large loop. Then, there is a π phase shift between the two ends of the s-wave superconductor. This is a new way to realize the π junction[71] by inserting a two-band superconductor with $s\pm$ pairing symmetry between two conventional s-wave superconducting electrodes. For a superconducting loop containing a π junction, TRSB occurs with a spontaneous magnetic flux of $\Phi_0/2$. If this spontaneous magnetic flux is measured, then it can unequivocally prove the sign-reversal pairing symmetry for the two-band superconductors.

The above analysis can be generalized into Josephson junctions in grain boundaries of $s\pm$ multiband superconductors. As shown in Fig. 8(b), there are four tunneling channels in the grain-boundary junction, with two diagonal and two off-diagonal tunnelings. The total energy can be written as

$$E = -J_{t11}\cos(\theta_{t1} - \theta_{b1}) - J_{t12}\cos(\theta_{t1} - \theta_{b2})$$
$$- J_{t21}\cos(\theta_{t2} - \theta_{b1}) - J_{t22}\cos(\theta_{t2} - \theta_{b2})$$
$$- J_t\cos(\theta_{t1} - \theta_{t2}) - J_b\cos(\theta_{t1} - \theta_{t2}), \quad (82)$$

where $J_{t\alpha\beta} > 0$ with α, $\beta = 1$, 2 are the interjunction couplings, and $J_t < 0$, $J_b < 0$ are interband couplings. For $|J_t|$ and $|J_b| \gg J_{t\alpha\beta} > 0$, $\theta_{t1} = \theta_{t2} + \pi$ and $\theta_{b1} = \theta_{b2} + \pi$, then the Josephson energy is simplified into

$$E = (-J_{t11} - J_{t22} + J_{t12} + J_{t21})\cos(\theta_{t2} - \theta_{b2}). \quad (83)$$

If at some part of the junction $(-J_{t11} - J_{t22} + J_{t12} + J_{t21}) > 0$, while at other part $(-J_{t11} - J_{t22} + J_{t12} + J_{t21}) < 0$, then we have exactly the same situation as studied in Eqs. (73) and (74). Spontaneous magnetic flux will appear in the grain boundary if this condition holds.

We then investigate the response of a junction in the TRSB state when spatial inhomogeneities of the Josephson couplings are present. In the TRSB state, ϕ_{si} depends on the Josephson couplings. The inhomogeneities induce variation of ϕ_{si}, and thus create magnetic field. We assume a weak defect in the J_{s2} channel $J_{s2} = \bar{J}_{s2} + \Delta_{s2}(x)$, and the response is $\phi_{si} = \bar{\phi}_{si} + \varphi_{si}$ with $\Delta_{s2} \ll 1$ and $\varphi_{si} \ll 1$. For simplicity, we assume two channels are identical $\zeta_1 = \zeta_2 = \zeta_s = \zeta$, $\bar{J}_{s2} = J_{s1}$, and $\bar{\phi}_{s2} = -\bar{\phi}_{s1} = \phi_0$. By substituting these expressions into Eqs. (22) and (26) and then expanding to the linear order, we have

$$\frac{\partial_x^2 \varphi_{s1} + \partial_x^2 \varphi_{s2}}{3\zeta + 2} = \cos\phi_0 \varphi_{s1} + \Delta_{s2}(x)\sin\phi_0 + \bar{J}_{s2}\varphi_{s2}\cos\phi_0,$$
(84)

$$-\frac{3\zeta + 1}{3\zeta + 2}\frac{\partial_x^2 \varphi_{s1}}{\zeta} + \frac{\partial_x^2 \varphi_{s2}}{\zeta(3\zeta + 2)} + 2\cos\phi_0\varphi_{s1} + \Delta_{s2}(x)\sin\phi_0$$
$$+ \bar{J}_{s2}\cos\phi_0\varphi_{s2} + J_{12}\cos(2\phi_0)(\varphi_{s1} - \varphi_{s2}) = 0.$$
(85)

Equations (84) and (85) can be solved in the Fourier space and the solution is given by

$$\varphi_{s1}(k) = -\frac{\sin\phi_0[2k^2(1+\zeta) + p^2(2+3\zeta) - q^2\zeta]}{(k^2 + p^2)(k^2 + q^2)}\Delta(k),$$
(86)

$$\varphi_{s2}(k) = -\frac{\sin\phi_0[2k^2(1+2\zeta) + p^2(2+3\zeta) + q^2\zeta]}{2(k^2 + p^2)(k^2 + q^2)}\Delta(k),$$
(87)

with $p^2 = [\cos\phi_0 + 2\cos(2\phi_0)J_{12}]\zeta$ and $q^2 = \cos\phi_0(2 + 3\zeta)$. We assume a point defect $\Delta(x) = \Delta_0\delta(x)$. Then, we obtain the induced modulation of phase in real space

$$\varphi_{s1}(x) = -\frac{\Delta_0\sin\phi_0}{4}\left[\frac{e^{-q|x|}q}{\cos\phi_0} - \frac{e^{-|x|p}p}{\cos\phi_0 + 2\cos(2\phi_0)J_{12}}\right],$$
(88)

$$\varphi_{s2}(x) = -\frac{\Delta_0\sin\phi_0}{4}\left[\frac{e^{-q|x|}q}{\cos\phi_0} + \frac{e^{-|x|p}p}{\cos\phi_0 + 2\cos(2\phi_0)J_{12}}\right],$$
(89)

FIG. 10. (Color online) Profile of the phases and magnetic field with a Gaussian-type defect $J_{s2}(x) = 1 - 0.4\exp[-(x - L/2)^2]$ in the Josephson coupling in a junction with $s\pm$ pairing symmetry obtained by numerical calculations. (a) and (b) correspond to two TRSB pair states. Inset is the phase configuration in the ground state. For clarity, the magnetic field is amplified by 20 times.

and the associated magnetic flux is given by

$$B = \frac{2\Delta_0\sin\phi_0\text{sign}[x]}{3\zeta + 2}\frac{e^{-|x|q}q^2}{4\cos\phi_0}.$$
(90)

Please note that the magnetic flux is singular at $x = 0$ because of the δ function used for the defects. Since Eqs. (88)–(90) all contain $\sin\phi_0$, the response to the same defect for distinct TRSB state differs by a sign, as shown in Figs. 9(a) and 9(b). This can be understood by looking at the phases of the three condensates. We have the freedom to fix the phase of the s-wave superconductor $\theta_s = 0$. As shown in the inset of Fig. 9(a), when J_{s2} is suppressed due to the local defect, the attraction between θ_s and θ_2 decreases, thus θ_2 decreases (rotates leftwards). As a result, θ_1 also decreases because the repulsion between θ_1 and θ_2 is reduced. The width of the region of phase variation is optimized by energy cost due to the phase gradient. While for the other TRSB ground state shown in Fig. 9(b), when J_{s2} decreases, θ_2 increases (rotates rightwards) as a result of the reduced attraction. Meanwhile, θ_1 also increases.

For a strong defect, we calculate the phases and magnetic field numerically. We model the point defect by a Gaussian distribution, and the results are presented in Fig. 10. Magnetic flux is induced near the defect, but the integrated magnetic flux in the junction vanishes. Meanwhile, the response for two
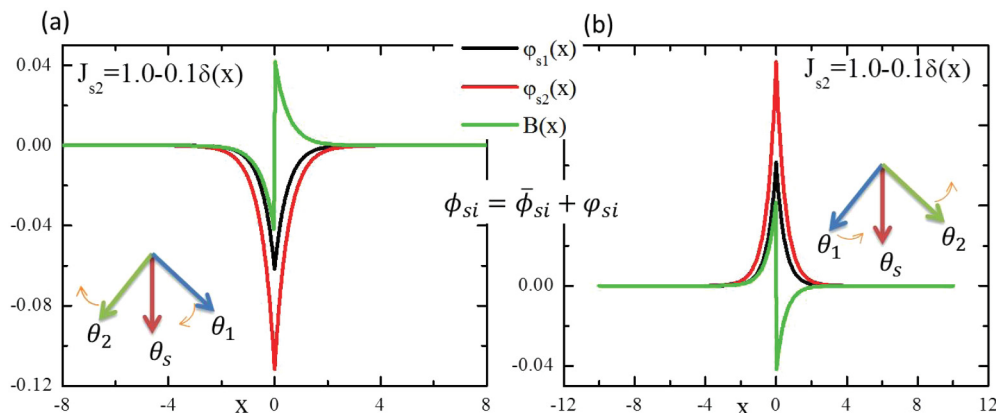

FIG. 9. (Color online) Profile of the phases and magnetic field with a defect in the junction with $s\pm$ pairing symmetry obtained from Eqs. (88)–(90). The defect is modeled as inhomogeneous Josephson coupling in the junction. (a) and (b) correspond to two TRSB pair states. Inset is the phase configuration in the ground state.
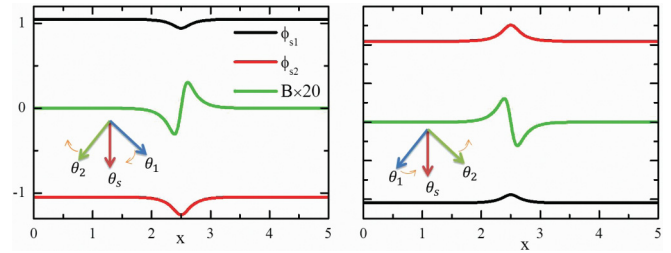
distinct TRSB states is different, consistent with the analytical results in Eqs. (88)–(90).

XIII. CONCLUSIONS

In this work, we have studied systematically the Josephson effect between a two-band superconductor and a conventional s-wave superconductor. We consider both the $s++$ and $s\pm$ pairing symmetries for the two-band superconductor. Due to the multiband nature of the superconducting electrode, there are two tunneling channels in the junction, which give rise to complicated interference in physical quantities, depending on the underlying pairing symmetry. Moreover, for junctions with $s\pm$ pairing symmetry, there exists frustrated interaction among different condensates, and under appropriate conditions, time-reversal symmetry is broken. Depending on the competition of interjunction Josephson couplings and interband Josephson coupling, the interference between the two tunneling channels can change continuously from adding constructively where they have the same phase to canceling destructively where they have a π phase shift. The interference manifests itself in the critical current, Shapiro steps, Fiske current steps, and Eck current steps.

In the case of thin superconducting electrodes, charge neutrality can be broken in the electrodes. Because of the charge neutrality breaking, out-of-phase oscillations of the gauge-invariant phase difference between two channels are possible, which gives a new plasma mode, in addition to the in-phase plasma oscillations. The energy gap of the out-of-phase mode vanishes at the time-reversal-symmetry breaking transition, which is an example of massless plasma mode in superconductors. Because of the existence of two plasma modes, there are additional Fiske and Eck resonances in the Josephson flux-flow region.

A long junction supports topological excitation of solitons. When the gauge-invariant phase difference associated with one tunneling channel changes by multiple 2π that is different from the change of phase difference in the other channel, fractional quantized magnetic solitons are stabilized in the junction. In contrast to the fractional vortices in bulk multiband superconductors, the fractional solitons have finite energy, thus are thermodynamically stable. For junctions with time-reversal-symmetry breaking, a new type of soliton excitations can be created between two distinct time-reversal pair states.

Finally, we showed that in junctions with time-reversal-symmetry breaking, disorders induce magnetic flux in the junctions, which points a unique way to detect the pairing symmetry of multiband superconductors.

*szl@lanl.gov

[1] B. D. Josephson, Phys. Lett. **1**, 251 (1962).

[2] A. Barone and G. Paterno, *Physics and Applications of The Josephson Effect* (Wiley, New York, 1982).

[3] V. B. Geshkenbein, A. I. Larkin, and A. Barone, Phys. Rev. B **36**, 235 (1987).

[4] C. C. Tsuei and J. R. Kirtley, Rev. Mod. Phys. **72**, 969 (2000).

[5] A. A. Golubov, M. Y. Kupriyanov, and E. Il'ichev, Rev. Mod. Phys. **76**, 411 (2004).

[6] J. Nagamatsu, N. Nakagawa, T. Muranaka, Y. Zenitani, and J. Akimitsu, Nature (London) **410**, 63 (2001).

[7] Y. Kamihara, T. Watanabe, M. Hirano, and H. Hosono, J. Am. Chem. Soc. **130**, 3296 (2008).

[8] X. X. Xi, Rep. Prog. Phys. **71**, 116501 (2008).

[9] K. Ishida, Y. Nakai, and H. Hosono, J. Phys. Soc. Jpn. **78**, 062001 (2009).

[10] J. Paglione and R. L. Greene, Nat. Phys. **6**, 645 (2010).

[11] D. C. Johnston, Adv. Phys. **59**, 803 (2010).

[12] H.-H. Wen and S. Li, Annu. Rev. Condens. Matter Phys. **2**, 121 (2011).

[13] F. Wang and D.-H. Lee, Science **332**, 200 (2011).

[14] P. J. Hirschfeld, M. M. Korshunov, and I. I. Mazin, Rep. Prog. Phys. **74**, 124508 (2011).

[15] G. R. Stewart, Rev. Mod. Phys. **83**, 1589 (2011).

[16] I. I. Mazin, D. J. Singh, M. D. Johannes, and M. H. Du, Phys. Rev. Lett. **101**, 057003 (2008).

[17] K. Kuroki, S. Onari, R. Arita, H. Usui, Y. Tanaka, H. Kontani, and H. Aoki, Phys. Rev. Lett. **101**, 087004 (2008).

[18] H. Ding, P. Richard, K. Nakayama, K. Sugawara, T. Arakane, Y. Sekiba, A. Takayama, S. Souma, T. Sato, T. Takahashi, Z. Wang, X. Dai, Z. Fang, G. F. Chen, J. L. Luo, and N. L. Wang, Europhys. Lett. **83**, 47001 (2008).

[19] L. Wray, D. Qian, D. Hsieh, Y. Xia, L. Li, J. G. Checkelsky, A. Pasupathy, K. K. Gomes, C. V. Parker, A. V. Fedorov, G. F. Chen, J. L. Luo, A. Yazdani, N. P. Ong, N. L. Wang, and M. Z. Hasan, Phys. Rev. B **78**, 184508 (2008).

[20] K. Terashima, Y. Sekiba, J. H. Bowen, K. Nakayama, T. Kawahara, T. Sato, P. Richard, Y.-M. Xu, L. J. Li, G. H. Cao, Z.-A. Xu, H. Ding, and T. Takahashi, Proc. Natl. Acad. Sci. USA **106**, 7330 (2009).

[21] Y. Zhang, L. X. Yang, F. Chen, B. Zhou, X. F. Wang, X. H. Chen, M. Arita, K. Shimada, H. Namatame, M. Taniguchi, J. P. Hu, B. P. Xie, and D. L. Feng, Phys. Rev. Lett. **105**, 117003 (2010).

[22] X. H. Zhang, Y. S. Oh, Y. Liu, L. Q. Yan, K. H. Kim, R. L. Greene, and I. Takeuchi, Phys. Rev. Lett. **102**, 147002 (2009).

[23] Y. R. Zhou, L. Y. R., J. W. Zuo, R. Y. Liu, S. K. Su, G. F. Chen, J. L. Lu, N. L. Wang, and Y. P. Wang, arXiv:0812.3295.

[24] C. T. Chen, C. C. Tsuei, M. B. Ketchen, Z. A. Ren, and Z. X. Zhao, Nat. Phys. **6**, 260 (2010).

[25] A. Brinkman, D. Mijatovic, H. Hilgenkamp, G. Rijnders, I. Oomen, D. Veldhuis, F. Roesthuis, H. Rogalla, and D. H. A. Blank, Supercond. Sci. Technol. **16**, 246 (2003).

[26] X. X. Xi, Supercond. Sci. Technol. **22**, 043001 (2009).

[27] P. Seidel, Supercond. Sci. Technol. **24**, 043001 (2011).

[28] D. F. Agterberg, E. Demler, and B. Janko, Phys. Rev. B **66**, 214507 (2002).

[29] W. Q. Chen, F. J. Ma, Z. Y. Lu, and F. C. Zhang, Phys. Rev. Lett. **103**, 207001 (2009).

[30] D. Parker and I. I. Mazin, Phys. Rev. Lett. **102**, 227007 (2009).

[31] Y. Ota, M. Machida, T. Koyama, and H. Matsumoto, Phys. Rev. B **81**, 014502 (2010).

[32] Y. Ota, M. Machida, and T. Koyama, Phys. Rev. B **82**, 140509(R) (2010).

[33] Y. Ota, N. Nakai, H. Nakamura, M. Machida, D. Inotani, Y. Ohashi, T. Koyama, and H. Matsumoto, Phys. Rev. B **81**, 214511 (2010).

[34] T. K. Ng and N. Nagaosa, Europhys. Lett. **87**, 17003 (2009).

[35] V. Stanev and Z. Tesanovic, Phys. Rev. B **81**, 134522 (2010).

[36] E. Simanek, *Inhomogeneous Superconductors: Granular and Quantum Effects* (Oxford University Press, New York, 1994).

[37] Y. Ota, M. Machida, T. Koyama, and H. Matsumoto, Phys. Rev. Lett. **102**, 237003 (2009).

[38] A. Alexander and B. D. Simons, *Condensed Matter Field Theory* (Cambridge University Press, Cambridge, 2010).

[39] H. Suhl, Phys. Rev. Lett. **14**, 226 (1965).

[40] T. Koyama and M. Tachiki, Phys. Rev. B **54**, 16183 (1996).

[41] M. Machida, T. Koyama, and M. Tachiki, Phys. Rev. Lett. **83**, 4618 (1999).

[42] R. Kleiner, F. Steinmeyer, G. Kunkel, and P. Müller, Phys. Rev. Lett. **68**, 2394 (1992).

[43] J. Linder, I. B. Sperstad, and A. Sudbo, Phys. Rev. B **80**, 020503 (2009).

[44] W.-Q. Chen and F.-C. Zhang, Phys. Rev. B **83**, 212501 (2011).

[45] L. N. Bulaevskii and A. E. Koshelev, Phys. Rev. Lett. **97**, 267001 (2006).

[46] A. Brinkman, A. A. Golubov, and M. Y. Kupriyanov, Phys. Rev. B **69**, 214407 (2004).

[47] S. Shapiro, Phys. Rev. Lett. **11**, 80 (1963).

[48] M. Cirillo, N. Gronbech-Jensen, M. R. Samuelsen, M. Salerno, and G. V. Rinati, Phys. Rev. B **58**, 12377 (1998).

[49] A. J. Dahm, A. Denenstein, T. F. Finnegan, D. N. Langenberg, and D. J. Scalapino, Phys. Rev. Lett. **20**, 859 (1968).

[50] R. G. Mints and I. B. Snapiro, Phys. Rev. B **52**, 9691 (1995).

[51] G. Hechtfischer, R. Kleiner, A. V. Ustinov, and P. Müller, Phys. Rev. Lett. **79**, 1365 (1997).

[52] A. J. Leggett, Prog. Theor. Phys. **36**, 901 (1966).

[53] S. Z. Lin and X. Hu, Phys. Rev. Lett. **108**, 177005 (2012).

[54] M. Tinkham, *Introduction to Superconductivity* (McGraw-Hill, New York, 1996).

[55] R. Kleiner, T. Gaber, and G. Hechtfischer, Phys. Rev. B **62**, 4086 (2000).

[56] X. Hu and S. Z. Lin, Supercond. Sci. Technol. **23**, 053001 (2010).

[57] R. E. Eck, D. J. Scalapin, and B. N. Taylor, Phys. Rev. Lett. **13**, 15 (1964).

[58] M. D. Fiske, Rev. Mod. Phys. **36**, 221 (1964).

[59] J. H. Kim, B.-R. Ghimire, and H.-Y. Tsai, Phys. Rev. B **85**, 134511 (2012).

[60] K. L. Ngai, Phys. Rev. **182**, 555 (1969).

[61] S. Sakai, P. Bodin, and N. F. Pedersen, J. Appl. Phys. **73**, 2411 (1993).

[62] S. Sakai, A. V. Ustinov, H. Kohlstedt, A. Petraglia, and N. F. Pedersen, Phys. Rev. B **50**, 12905 (1994).

[63] A. V. Ustinov, H. Kohlstedt, M. Cirillo, N. F. Pedersen, G. Hallmanns, and C. Heiden, Phys. Rev. B **48**, 10614 (1993).

[64] N. Manton and P. M. Sutcliffe, *Topological Solitons* (Cambridge University Press, Cambridge, 2004).

[65] Y. Tanaka, Phys. Rev. Lett. **88**, 017002 (2001).

[66] S. Z. Lin and X. Hu, New J. Phys. **14**, 063021 (2012).

[67] V. Vakaryuk, V. Stanev, W. Lee, and A. Levchenko, arXiv:1203.4554.

[68] E. Babaev, Phys. Rev. Lett. **89**, 067001 (2002).

[69] S. Pagano, M. P. Soerensen, R. D. Parmentier, P. L. Christiansen, O. Skovgaard, J. Mygind, N. F. Pedersen, and M. R. Samuelsen, Phys. Rev. B **33**, 174 (1986).

[70] T. A. Fulton and R. C. Dynes, Solid State Commun. **12**, 57 (1973).

[71] L. N. Bulaevskii, V. V. Kuzii, and A. A. Sobyanin, Pis'ma Zh. Eksp. Teor. Fiz. **25**, 314 (1977) [JETP Lett. 25, 290 (1977)].